Available online at www.sciencedirect.com
SCIENCE DIRECT®
International Journal of Multiphase Flow 30 (2004) 1369–1388
International Journal of Multiphase Flow
www.elsevier.com/locate/ijmulflow

Numerical modeling and experimental measurements of a high speed solid-cone water spray for use in fire suppression applications

S.S. Yoon [a,*], J.C. Hewson [a], P.E. DesJardin [b], D.J. Glaze [c], A.R. Black [a], R.R. Skaggs [d]

[a] *Sandia National Laboratories, Fire Science and Technologies, P.O. Box 5800, Albuquerque, NM 87185-1135, United States*
[b] *Department of Mechanical and Aeronautical Engineering, University of Buffalo, Buffalo, NY 14260, United States*
[c] *Department of Mechanical Engineering, Purdue University, W. Lafayette, IN 47907, United States*
[d] *US Army Research Laboratory, AMSRL-WM-TB, Aberdeen Proving Ground, MD 21005-5066, United States*

Received 23 April 2004; received in revised form 28 July 2004

Abstract

Experimental measurements and numerical simulations of a high-speed water spray are presented. The numerical model is based on a stochastic separated flow technique that includes submodels for droplet dynamics, heat and mass transfer, and droplet–droplet collisions. Because the spray characteristics near the nozzle are difficult to ascertain, a new method for initialization of particle diameter size is developed that assumes a Rosin–Rammler distribution for droplet size, which correctly reproduces experimentally measured Sauter and arithmetic mean diameters. By relating the particle initialization to lower moments of the droplet statistics, it is possible to take advantage of measurements without substantial penalties associated with the greater experimental uncertainty of individual droplet measurements. Overall, very good agreement is observed in the comparisons of experimental measurements to computational predictions for the streamwise development of mean drop size and velocity. In addition, the importance of modeling droplet–droplet collisions is highlighted with comparison of selected droplet–droplet collision models.

* Corresponding author. Tel.: +1 505 284 8400; fax: +1 505 845 3151.
E-mail address: ssyoon@sandia.gov (S.S. Yoon).

0301-9322/$ - see front matter © 2004 Elsevier Ltd. All rights reserved.
doi:10.1016/j.ijmultiphaseflow.2004.07.006

1. Introduction

Rapid fire suppression is a necessity for modern vehicle crew compartments and for enclosures containing critical equipment susceptible to fire damage. For these applications, high-momentum sprays are useful for quickly dispersing condensed-phase suppressants to the fire and the surrounding compartment to minimize the thermal insult to its occupants. The current paper focuses on the predictive modeling of a specific nozzle, typical of those that might be used to provide suppression in a compartment in a matter of seconds or less. Droplet size and velocity measurements are presented to help develop the appropriate initial conditions for this nozzle and to aid in evaluating the model.

One of the challenges in modeling the injection of these sprays is the initialization of the drop size and velocity using Lagrangian separated flow modeling approaches. The atomization process that occurs as the spray leaves the nozzle is particularly difficult to describe. Several authors (Yoon et al., 2004c; Widmann et al., 2001) reported the difficulty associated with the optical access in the region where countless droplets surrounding the exiting liquid slug (or core). High-resolution measurements and high-fidelity modeling (DesJardin and Gritzo, 2002) of the near-nozzle flow provide significant insight into the various processes in this region. Among the relevant processes are turbulent fluctuations in the condensed phase (Wu et al., 1991, 1992), shear driven (Kelvin–Helmholtz) instabilities (Reitz and Bracco, 1982; Wu et al., 1986), boundary layer effects (Hoyt and Taylor, 1977a,b; Yoon and Heister, 2003, 2004a,b) and cavitation (Bergwerk, 1959). While there has been extensive progress in this area, accurate prediction of the droplet initial conditions from a given nozzle geometry is not yet possible and therefore semi-empirical prescriptions of initial droplet size and velocity are required for numerical simulations of sprays.

The initial condition approach pursued in this study is a novel Monte Carlo sampling technique using a prescribed Rosin–Rammler distribution for drop size. Although there are distribution functions that can sometimes reproduce experimental measurements more accurately, it was found that the mathematical simplicity of the Rosin–Rammler distribution makes it a powerful tool for parameterizing initial conditions in terms of experimental measurements of the arithmetic and Sauter-mean diameters. In this paper, we describe the use of a spatially varying Rosin–Rammler distribution as an initial condition for spray simulations. The dispersion coefficient (q) and the mean diameter (X) for the distribution are extracted from the experimental data for the arithmetic mean diameter, D_{10}, and the Sauter mean diameter, D_{32}.

In the following sections, the modeling approach and experimental arrangement are summarized, with special attention on the initial and boundary conditions for prescribing the spray initial droplet size. Simulation results using this new inlet condition treatment are then presented and compared to the experimental measurements.

2. Experimental apparatus

The water spray used for the purpose of model evaluation is produced using a converging nozzle manufactured by *Spraying Systems Co.*, Wheaton, IL. The internal converging angle is

approximately 40°, and is followed by a constant-diameter section of length 3.31 mm as shown in Fig 1(a). The water spray is directed horizontally, as shown in Fig. 1(b), with a liquid core speed of $U = 80$ m/s, a diameter of $d = 2$ mm, a mass flow rate of $\dot{m} = 0.25$ kg/s, and a liquid and gas temperature of $T = 300$ K. The nondimensional parameters are $Re = Ud/v = 142{,}857$, $We = \rho U^2 d/\sigma = 174{,}387$, $We_g = \rho_g U^2 d/\sigma = 215$, and $Oh = \mu/\sqrt{\rho d \sigma} = 0.0023$. Since $We_g > 40$, the spray is in the atomization regime (Reitz, 1978).

Radial profiles of particle sizes and axial velocities were measured with a Phase Doppler Particle Analyzer (PDPA) at the Army Research Laboratories. Measurements were conducted at four axial locations, beginning at $x = 48$ mm and continuing to $x = 250$, 480, and 810 mm downstream of the spray nozzle. These distances correspond to 24, 125, 240 and 405 in terms of distances normalized by the nominal nozzle diameter. Results are presented in terms of quantities averaged at a given downstream distance and radial location. At each location, data was collected for a fixed time, 5 s, in an attempt to determine the number density of particles at that location. We report results for radial locations where approximately 10,000 particles

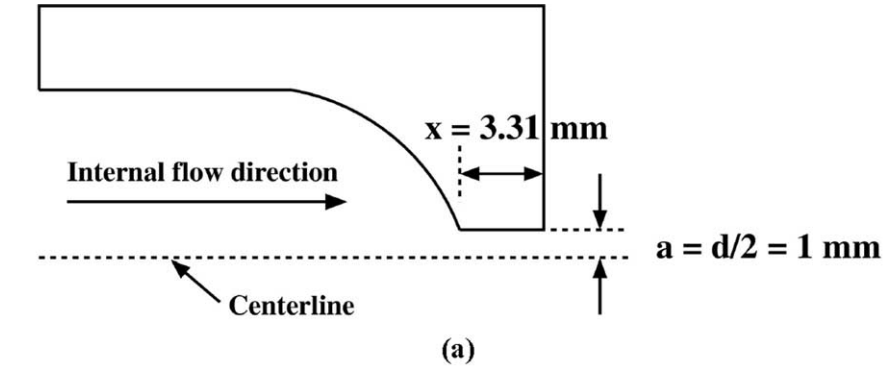

(a)

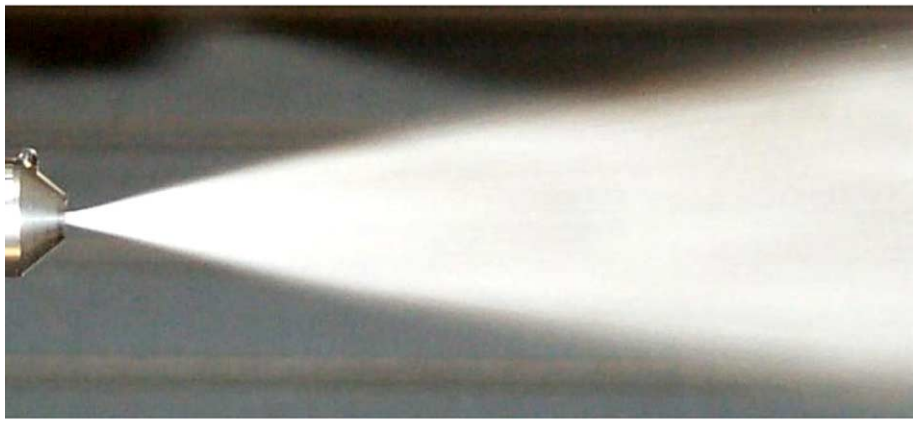

(b)

Fig. 1. (a) Schematic of the nozzle geometry, (b) Near-field view of the high-pressure water spray.

per second were counted; statistics at other locations are insufficient for reporting results. Uncertainties for the averaged particle diameters and velocities are estimated to be 10–15% in accordance with our experience; these uncertainties are likely dominated by systematic errors.

3. Computational model

Simulations are conducted using the Vulcan fire simulation code, which has been extended to handle the dilute multiphase flow physics found in evaporating and reacting sprays (DesJardin and Gritzo, 2002). The spray model is coupled with the Navier–Stokes solver, which is based on a Reynolds averaged Navier Stokes (RANS) formulation employing a standard k–ε turbulence closure model (Jones and Launder, 1972). The gas-phase flow is calculated on an Eulerian staggered Cartesian grid using the SIMPLEC method (Patankar, 1980).

The condensed phase evolves using a Lagrangian approach based on the stochastic separated flow model (Faeth, 1983, 1987). Evolution equations for collections of droplets with similar sizes and initial conditions, denoted as parcels, are used to reduce computational cost. A sufficient number of parcels are used to ensure an adequate resolution of the spray physics and the measured droplet statistics. Statistical variations in droplet size and velocity are imposed as initial conditions to simulate the liquid jet breakup process, of which phenomenon was experimentally shown by Sallam and Faeth (1999) and Sallam et al. (2002). The parcels are advanced under the influence of modeled turbulent fluctuations in the gas-phase properties.

3.1. Conservation of mass

The correlation by Ranz and Marshall (1952a,b) is used for the evaporation model,

$$\frac{\mathrm{d}m}{\mathrm{d}t} = \pi D \frac{\mu_\mathrm{f}}{Sc_\mathrm{f}} \left[2 + \frac{2}{3} Re^{1/2} Sc_\mathrm{f}^{1/3} \right] \ln(1 + B_\mathrm{m}) \tag{1}$$

where m is the droplet mass, D is the droplet diameter, $Sc_\mathrm{f} = \nu_\mathrm{f}/D_\mathrm{M}$ is the film Schmidt number, D_M is the mass diffusivity, $Re = \rho_\mathrm{g} d \mid \vec{u}_\mathrm{p} - \vec{u}_\mathrm{g} \mid /\mu_\mathrm{g}$ is the droplet Reynolds number, and $B_\mathrm{m} = (Y_\mathrm{f} - Y_\mathrm{g})/(1 - Y_\mathrm{f})$ is the Spaulding or mass transfer number that characterizes the concentration gradients at the film interface. In these and all subsequent expressions, the subscripts $()_\mathrm{g}$ represent gas properties, $()_\mathrm{d}$ represent droplet properties, and $()_\mathrm{f}$ represent droplet film properties for the thin-film approximation of the liquid–gas interface at the droplet surface.

3.2. Conservation of momentum

The momentum equation for a small rigid sphere in a non-uniform flow is derived by Maxey and Riley (1983). As discussed by Faeth (1987), if the ratio of particle to gas densities is large (i.e. $\rho_\mathrm{l}/\rho_\mathrm{g} \gg 1.0$) then the predominant forces generally consist of the drag and body forces leading to a relatively simple form of the momentum equation,

$$m\frac{\mathrm{d}u_{\mathrm{D}}}{\mathrm{d}t}=\frac{\pi}{8}\rho_{\mathrm{g}}D^2C_{\mathrm{D}}\mid\vec{u}_{\mathrm{g}}-\vec{u}_{\mathrm{D}}\mid(\vec{u}_{\mathrm{g}}-\vec{u}_{\mathrm{D}})+mg \tag{2}$$

where $\vec{u}_{\mathrm{D}}$ is the droplet velocity and $\vec{u}_{\mathrm{g}}$ is the gas phase velocity around that particle and ρ_{g} is the gas phase density. The last term on the right hand side is the body force term due to gravity. The coefficient of drag, C_{D} is modeled using the standard drag coefficient relations for a sphere in a uniform flow (Faeth, 1987; Maxey and Riley, 1983).

3.3. Conservation of energy

The droplet temperature evolution is a balance between convection and evaporation. The droplet thermal energy can then be expressed as

$$mc_{\mathrm{v,d}}\frac{\mathrm{d}T}{\mathrm{d}t}=\dot{Q}_{\mathrm{c}}+\dot{Q}_{\mathrm{e}} \tag{3}$$

where

$$\dot{Q}_{\mathrm{c}}=\pi d\frac{\mu_{\mathrm{f}}}{Pr_{\mathrm{f}}}c_{\mathrm{p,f}}(T_{\mathrm{g}}-T)\left[2+\frac{k}{F(B_{\mathrm{t}})}Re^{1/2}Pr_{\mathrm{f}}^{1/3}\right]\frac{\ln(1+B_{\mathrm{t}})}{B_{\mathrm{t}}},$$

$$\dot{Q}_{\mathrm{e}}=\dot{m}h_{\mathrm{v,f}}$$

In these expressions, $Pr_{\mathrm{f}}=v_{\mathrm{f}}/\alpha_{\mathrm{f}}=c_{\mathrm{p,f}}\mu_{\mathrm{f}}/k_{\mathrm{f}}$ is the film Prandtl number and $h_{\mathrm{v,f}}$ is the heat of vaporization. A "thin-skin" model is used and conditions at the droplet surface are obtained iteratively by equating heat flux to the droplet with droplet heating and enthalpy associated with vaporization (Faeth, 1987). The relationship between the quasi-steady state film temperature and the fluxes to the droplet are modeled by the Spaulding heat transfer number, $B_{\mathrm{t}}=[1+B_{\mathrm{m}}]^{Le_{\mathrm{f}}}-1$.

3.4. Collision, breakup, and turbulence models

Droplet–droplet collisions occur during the atomization of a liquid jet. For some applications, accounting for these collisions may be important in reproducing observed mean drop sizes downstream of primary atomization. Collisions of pairs of computational parcels are treated using a statistical process description. The procedure starts by checking to see if two parcels occupy the same computational cell. If they do not share the same cell then it is assumed that collisions cannot occur. If they do share the same cell then the parcel containing the larger drops are designated as the collectors and parcel containing the smaller drops designated as the donors. The expected frequency of collisions between by one collector with all the droplets is assumed to obey the collision-criteria suggested by Ko et al. (2003). This approach only accounts for either droplet–droplet 'bouncing' or 'coalescence', and not droplet–droplet 'shattering' effect that produces additional drops. The 'shattering' effect may become important for the head-to-head colliding sprays (Georjon and Reitz, 1999). Since all droplets are moving in the same direction in our spray, the "shattering" is highly unlikely to occur. The Taylor Analogy Breakup (TAB) Model of O'Rourke and Amsden (1987) is adopted to indicate the significance of droplet breakup in this study. The model assumes a direct analogy between the oscillation of a droplet and a forced spray-mass-damper system (O'Rourke and Amsden, 1987).

Turbulence models are introduced at the parcel and sub-parcel level to account for the effect of local fluctuations in the velocity field while the rest of the thermo-physical variables are approximated by their corresponding time averaged values. The velocity-fluctuation models serve to increase the droplet dispersion, mimicking the effects of unresolved turbulent eddies. These unresolved turbulent motions are significant for the present high-pressure spray that generates substantial turbulent kinetic energy. These unresolved turbulent motions are decomposed into parcel and sub-parcel models.

The parcel turbulence model accounts for the effects of turbulent eddies perturbing the parcel trajectory and is based on the random walk model of Gosman and Ioannides (1981), as modified by Shuen et al. (1983). This model essentially perturbs the gas velocity $\vec{u}_g$ in Eq. (2) by an amount randomly selected from a Gaussian distribution over the velocity scales expected based on the turbulent kinetic energy.

Within a parcel, the spatial distribution of particles is assumed to be of Gaussian form. The standard deviation of this spatial distribution evolves with time for each parcel at a velocity, $\vec{u}'_p$, with the evolution equation for $\vec{u}'_p$ being essentially Eq. (2) except that the velocities are replaced by $\vec{u}'_p$ and the fluctuating gas velocity in the manner of Zhou and Yao (1992); the buoyant term is also neglected in particle dispersion since it acts equally on all particles.

3.5. Initial conditions

To represent conditions at the nozzle exit, presumed-shape droplet size and velocity distributions are often used. There are many known droplet size distribution functions such as normal, log-normal, root-normal, Rosin–Rammler, Nukiyama-Tanasawa, and log-hyperbolic (Babinsky and Sojka, 2002). For the majority of the simulations presented here, initial droplet sizes at the injector location are chosen from prescribed PDF's using the Rosin–Rammler distribution. The Rosin–Rammler cumulative distribution function (CDF) is:

$$\mathrm{CDF} = \int_0^D f(D)\,\mathrm{d}D = 1 - \exp\left[-\left(\frac{D}{X}\right)^q\right] \tag{4}$$

where

$$f(D) = \frac{qD^{q-1}}{X^q}\exp\left[-\left(\frac{D}{X}\right)^q\right] \tag{5}$$

so that the droplet diameter is obtained using a uniformly distributed random number, RN, with

$$D = X[\ln(1-\mathrm{RN})^{-1}]^{\frac{1}{q}} \tag{6}$$

where X represents characteristic droplet size and q is an empirical dimensionless constant to specify the distribution width, sometimes referred to as the dispersion coefficient. It should be noted that the parcel size distribution will differ from the above particle size distribution as shown in Fig. 2.

There is a factor of D^3 difference between the size distribution PDF of individual particles and modeled parcels of particles, $f(D)_{\mathrm{parc}} = D^3 f(D)_{\mathrm{part}}$, because the submodel parameter, PPP (number of particles per parcel) is based on a fixed mass per parcel which weights the droplet distribution

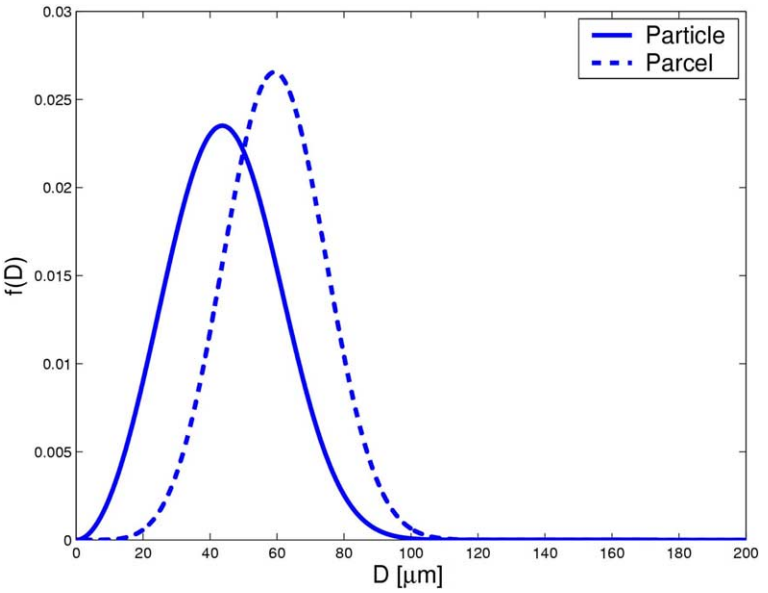

Fig. 2. Comparison of size distribution for individual particles and parcels of particles, for $q = 3$ and $X = 50\,\mu\text{m}$.

by a factor proportional to $1/D^3$ (i.e. PPP $= \dot{m}_{\text{total}}(\Delta t_{\text{inj}}$ per parcel$)/m_{\text{part}}$), as shown in Fig. 2. To obtain the desired particle size distribution, it is the scaled parcel distribution that must be implemented in the spray model. This difference by a factor of D^3 yields the following parcel distribution:

$$\text{CDF}_{\text{parc}} = \frac{1}{N}\int_0^D f(D)_{\text{parc}}\,\mathrm{d}D \tag{7}$$

$$\text{where } f(D)_{\text{parc}} = D^3\frac{qD^{q-1}}{X^q}\exp\left[-\left(\frac{D}{X}\right)^q\right] \tag{8}$$

Here, N is a normalization factor, which is evaluated as follows:

$$N = \int_0^\infty f(D)_{\text{parc}}\,\mathrm{d}D = X^3\Gamma\left(\frac{3}{q}+1\right) \tag{9}$$

Substituting Eqs. (7) and (8) into Eq. (9) yields the incomplete Gamma function, $P(3/q+1, D^{*q})$, where D^{*q} is the non-dimensional diameter defined as $D^* = D/X$. In general, the incomplete Gamma function is defined as (Press et al., 1992):

$$\text{CDF} = P(a,x) = \frac{1}{\Gamma(a)}\int_0^x \exp(-t)t^{a-1}\,\mathrm{d}t \tag{10}$$

Its inverse function can be obtained using the algorithm developed by Didonato and Morris (1986) with the given inputs, a $(=3/q+1)$ and $P(a,x)$. Solving for x is equivalent to solving for $D^* = x^{1/q}$.

The moments of the Rosin–Rammler drop-size distribution can be expressed as

$$\int_0^\infty D^n f(D)_{\mathrm{RR}}\,\mathrm{d}D = X^n \Gamma\left(\frac{n}{q}+1\right) \tag{11}$$

With this Eq. (11), the algebraic and Sauter-mean diameters can be parameterized in terms of the Rosin–Rammler parameters X and q. The mean diameter, D_{10}, is written as:

$$D_{10} = X\Gamma\left(\frac{1}{q}+1\right) \tag{12}$$

Similarly, the Sauter Mean Diameter (SMD) can be written as:

$$D_{32} = \frac{X^3\Gamma\left(\frac{3}{q}+1\right)}{X^2\Gamma\left(\frac{2}{q}+1\right)} \tag{13}$$

The variation of D_{32}, D_{10}, and their ratio as a function of the dispersion coefficient, q, in the Rosin–Rammler distribution is shown in Fig. 3. The locus of points defined by the curves in Fig. 3 allow one to identify X and q given D_{10} and D_{32}, both of which are relatively easy to obtain exper-

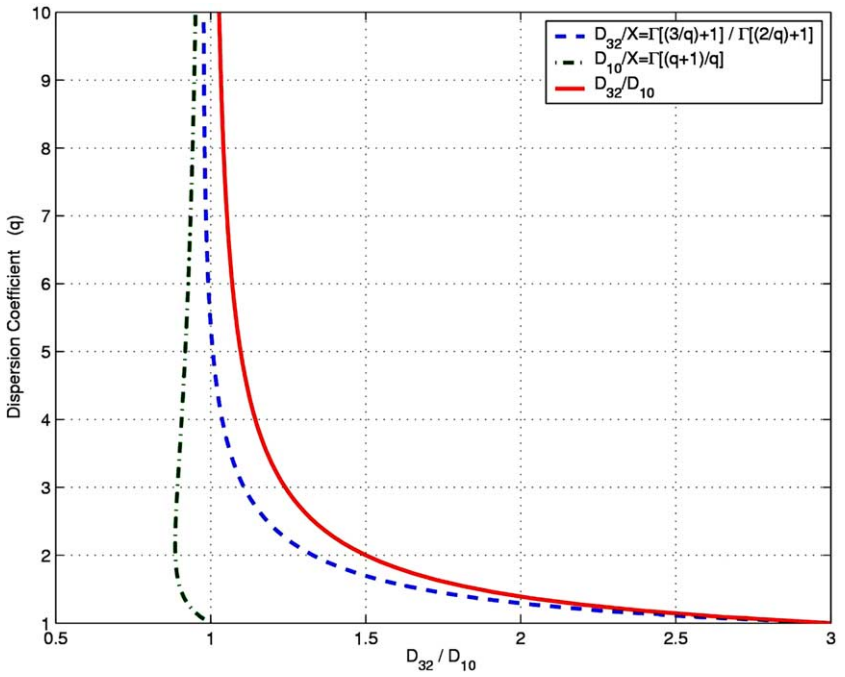

Fig. 3. Analytical expressions of average droplet size (D_{10}), Sauter Mean Diameter (D_{32}), and their ratio with the given Rosin–Rammler distribution function.

imentally. The dispersion coefficient is first identified from the ratio D_{32}/D_{10} and X is then determined from either D_{10} or D_{32}. Note that X is not equivalent to D_{10} except when q is unity or infinity. The dispersion coefficient, q, can be obtained as a function of the radial location when D_{32} and D_{10} are provide by experimental measurements.

There is an additional difficulty in using the presumed shape distribution parameterized by various measured mean diameters. The difficulty arises because the initial jet breakup occurs over a finite distance so quantities such as D_{10} and D_{32} are not well defined too close to the nozzle. Furthermore, the numerous droplets in this region obscure the optical access and, thus, it does not allow sufficiently accurate measurements. To overcome this difficulty, we have taken measurements as close to the nozzle as reliably possible, at 48 mm downstream, and used these to define our initial droplet distribution at that location. As will be discussed in Section 4, even at this location, there is substantial radial variation in the droplet size distribution. To account for the radial variation in the droplet size distribution, the injection is provided as a series of concentric injections at the radii corresponding to the measurements, with an appropriate flow angle. The mass flow rate at each radial location is made proportional to the experimentally measured mass flow rate. The measured flow rate is determined to be proportional to the number of particles passing through the probe volume multiplied by their average axial velocity times their mass appropriately weighted by the number of particles passing through the probe volume of the concentric injections. The parameters selected for the Rosin–Rammler distributions will be presented in the following section along with the data on which they are based.

An alternative approach is to extrapolate the droplet distribution parameters back to the nozzle and use the presumed Rosin–Rammler distribution as the initial condition at the nozzle location; this approach will be discussed in Section 4.

3.6. Computation details

All simulations run for a duration of two seconds on a $1.2\,\mathrm{m} \times 0.8\,\mathrm{m} \times 0.8\,\mathrm{m}$ domain. A $52 \times 43 \times 43$ cartesian grid is employed, except for the grid sensitivity study presented later, with grid stretching employed to enhance the resolution nearer the spray. The flow is essentially steady after 0.2 s and statistics are collected from 0.2 to 2.0 s at intervals of 0.0002 s. Parcels are injected at a rate of 133,333 per sec; the average mass associated with each parcel is approximately 1.875×10^{-6} kg of water. The number of droplets per parcel is dependent on the droplet diameter, as determined in the previous section, and sufficient to account for the initial mass associated with the parcel.

4. Experimental and simulation results

Measurements of the droplet diameters and velocities were obtained as a function of radial location using the PDPA at four downstream locations. We first report measurements at the first location, 48 mm, which are used as initial conditions for the simulation. We then report measurements and simulation results at further downstream locations.

4.1. Measurements near the nozzle

The downstream location closest to the nozzle at which measurements could reliably be made is 48 mm. Measurements there at five radial locations are presented in Table 1. The arithmetic mean diameters are in the range of 30–55 μm. This data along with the known flow rate, nozzle characteristics, and results of the analysis in Yoon and Heister (2004a) can be used to characterize the initial jet breakup. The particular converging nozzle geometry selected is known to minimize liquid turbulence in the approach to the nozzle orifice, but a low level of turbulent fluctuations will remain. These turbulent fluctuations can lead to internal boundary layer growth and developing turbulence. Yoon and Heister (2004a) show that the critical Weber number, $We_t = \rho U^2 \delta_2 / (\sigma Re_{\delta_2}^{1/2})$, for the breakup to be characterized as turbulent is roughly 20 for this type of nozzle. Here, ρ is the liquid density, U is the bulk flow velocity, δ_2 is the momentum thickness, σ is the surface tension and Re_{δ_2} is the Reynolds number based on U and δ_2. A conservative analysis assuming that the boundary-layer growth starts at the corner between the converging nozzle and constant-diameter section of the nozzle leads to an estimated Weber number for the jet of 22. This is just above the critical value for the transition to turbulent jet breakup identified in Fig. 11 of Yoon and Heister (2004a). Further, the ratio between the mean droplet diameter and the nozzle diameter, on the order of 0.025, falls close to the turbulent limit observed in Yoon and Heister (2004a). Therefore, we can characterize this breakup process as a predominantly turbulent breakup process.

Two trends for the droplet diameter as a function of radius are evident in the measurements at 48 mm. First, the average diameter increases with radial location. The variation of the mean diameter with radial location will be discussed in the following section along with results from other downstream locations. Second, the shape of the droplet diameter distribution changes, as is indicated by the changes in the ratio D_{32}/D_{10}. The effect of this on the droplet distribution is best shown through the droplet diameter distributions that are plotted in Fig. 4. In Fig. 4, it is evident that there are a larger number of small droplets along the centerline, leading to the smaller arithmetic mean. As the radius increases, the droplet distribution appears less skewed, with a reduced number of smaller particles at larger radii. Also shown in Fig. 4 are the Rosin–Rammler distributions, used to initialize the spray, that are obtained for the values of D_{32} and D_{10} shown in Table 1. The agreement between the Rosin–Rammler distribution and the measured droplet size distribution is quite reasonable; the greatest discrepancy is the inability of the Rosin–Rammler distribution to reproduce the sharper peak along the spray centerline. In the simulations, the droplet sizes

Table 1
Experimental data and model parameters at $x = 48$ mm

y [mm]	0	5	10	15	20
D_{10} [μm]	32.29	43.33	43.08	43.86	54.76
D_{32} [μm]	68.92	71.19	69.71	64.95	71.19
D_{32}/D_{10}	2.134	1.643	1.618	1.481	1.300
q	1.288	1.747	1.784	2.043	2.651
$\Gamma(1/q+1)$	0.925	0.891	0.890	0.886	0.889
X [μm]	34.91	48.63	48.40	49.51	61.71
$\dot{m}$ [kg/s]	0.130	0.028	0.064	0.016	0.012

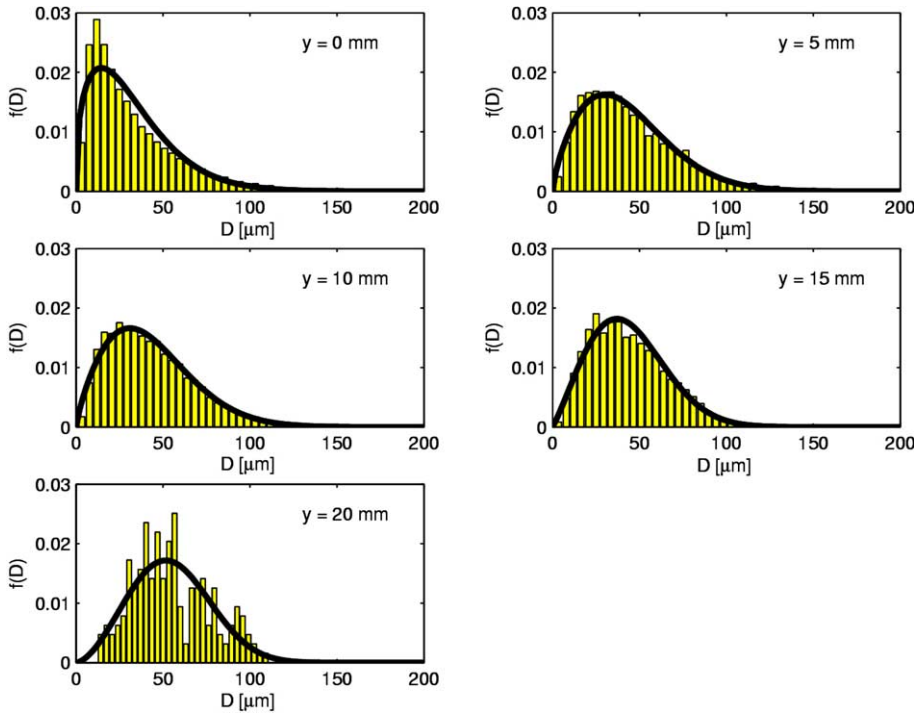

Fig. 4. Comparison of the droplet size distribution between Rosin–Rammler model (solid-line) and the experimental data (bar-graph) at $x = 48$ mm for various radial locations.

are randomly sampled from the distributions shown in Fig. 4 and parameterized in Table 1 using the techniques described in Section 3.5.

Another form of initial condition that we considered was the use of the measured droplet distribution. The reason that this method was not selected to provide the final simulation results are two-fold. First, the apparent noise in the distribution, especially at the radial location of 20 mm, is a concern. Second, data on moments of the diameter are much easier to obtain with good accuracy than are droplet size distributions. Therefore, we focus on the feasibility of using the presumed-shape distribution-function method because it is likely to be more generally applicable.

4.2. Liquid-core breakup length

As shown in Fig. 1(b), the fluid slug exiting the orifice is quickly atomized and generates numerous droplets; no lengthy slug of fluid is observed. The high Weber number (i.e. $We = 174{,}387$) is responsible for the behavior of a short liquid core. If the Weber number had been relatively low, the liquid core length (L_c) would have been extended (i.e., $L_c > 100$). Traditionally, the Rayleigh instability analyses (Rayleigh, 1878; Weber, 1931; McCarthy and Molloy, 1974; Sterling and Sleicher, 1975) are often used to predict the breakup length, L_c, approximated as $L_c \sim U/\omega_m$ where ω_m is the maximum growth rate. This type of approach is known to work reasonably well for low-speed jets. Sometimes, this method can also be applied to high-speed jets (Sallam and Faeth, 1999; Sallam et al., 2002; Hoyt and Taylor, 1977a) because the larger wavelengths are affected by

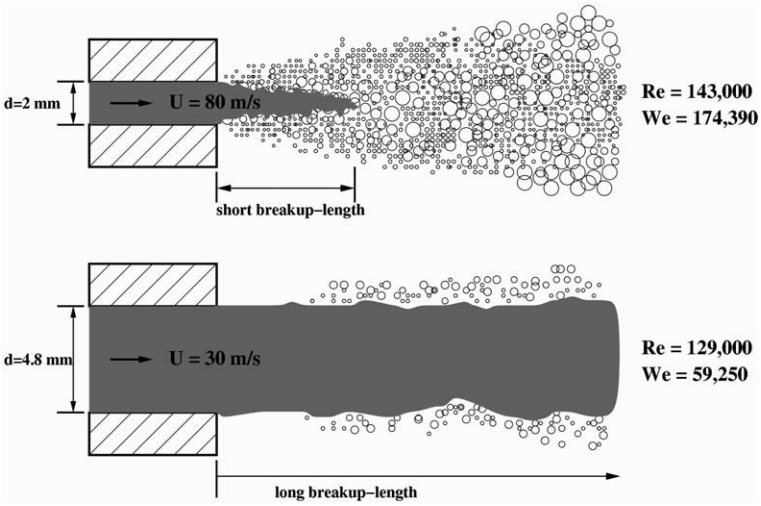

Fig. 5. Two different turbulent jets at different Weber number. (Above) Highly atomizing jet with short breakup length at "very" high Weber number; the jet investigated in this report. (Below) Moderately atomizing jet with long breakup length at moderately high Weber number; the jet investigated in Sallam et al. (2002).

Rayleigh instability while the smaller wavelengths are affected by other instability sources (i.e., Kelvin–Helmholtz type instability, boundary-layer instability, turbulence etc.). However, this method for estimating the jet breakup length is not applicable to "very" high-speed jets where the Weber number exceeds $We > 100{,}000$. The reasons are as follows: First, droplets are quickly formed and thus there is no lengthy liquid core. Second, there are no larger-scale disturbances; the small-scale disturbances dominate the flow physics, which cannot be predicted by the Rayleigh-type instability analysis. For these reasons, the breakup length of our jet is not comparable to the jet breakup length of Sallam et al. (2002). The liquid-core at very high Weber number (i.e. $We = 174{,}387$) is quite short (i.e. $L_c < 4$ or $5d$) while that of Sallam et al. is much longer (i.e. $L_c > 100d$). It is highly likely that the breakup length is scaled by the momentum thickness, δ_2, since the small-scale, which determines the overall droplet size, is comparable with δ_2 of the boundary layer instability (Yoon and Heister, 2004a). The schematic shown in Fig. 5 explains the difference between our very high-speed jet and Sallam et al.'s (2002) moderately high-speed jet.

5. Results and discussion

5.1. Downstream spray evolution

Measurements of D_{10} and U, the arithmetically averaged particle axial velocity, are shown at 250 mm, 480 mm, and 810 mm, downstream of the nozzle in Figs. 6 and 7 along with the data from 48 mm. Measurements can be compared with the simulation results in Figs. 6 and 7. In general the simulations agree well with the measurements, except for a slightly under-predicted spray cone angle. The local jet spreading rate greatly depends on the local turbulence modeling (Pope, 1978).

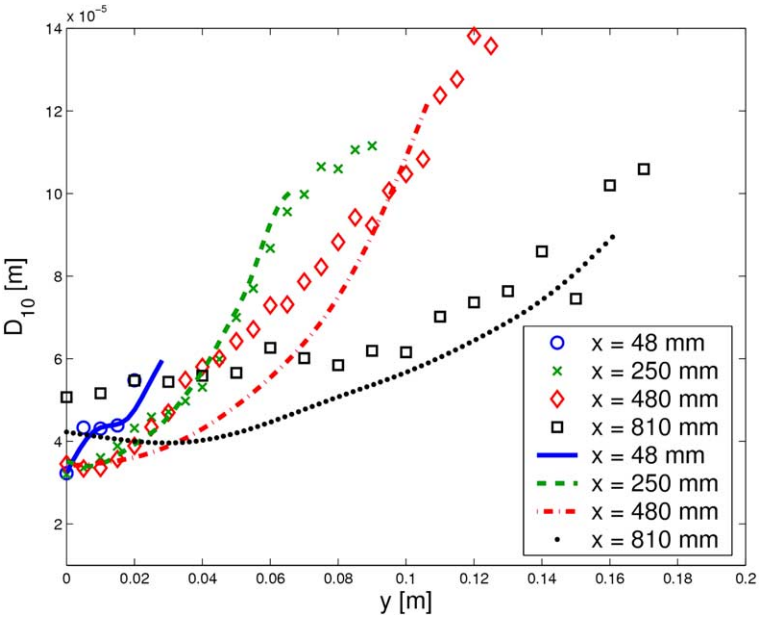

Fig. 6. Radial distributions of axial droplet size at various axial locations. Symbols are experimental data and lines are the computational results.

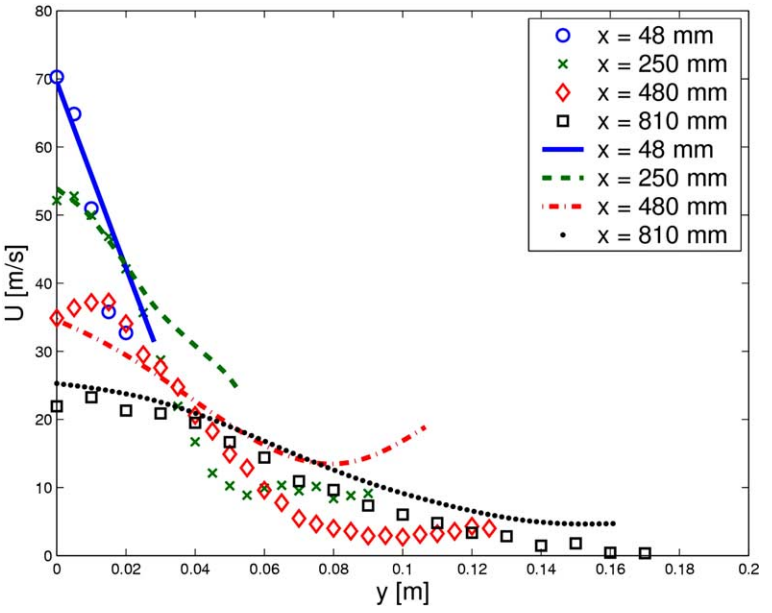

Fig. 7. Axial velocity distribution at various axial locations. Symbols are experimental data and lines are the computational results.

The model currently used has a shortcoming to predict the turbulent kinetic energy predicting (Pai and Subramaniam, 2004), which eventually leads to underprediction of the local jet spreading rate. From Figs. 6 and 7 the long time evolution of the spray can be observed. There is a clear segregation of the smaller particles in the inner region of the spray while larger particles are able to move to the outer regions of the spray. Thus the reduction in the number of smaller particles closer to the centerline observed in Fig. 4 continues throughout the majority of the spray evolution. However, at the farthest downstream distance measured, the distribution of droplets becomes substantially more uniform with radial location. The segregation of small droplets near the centerline can be attributed to the competition between turbulent dispersion and entrainment of air by the spray. Droplets that are dispersed by turbulent fluctuations will move outwards from the center, but their outward motion will be countered by the air entrainment. Air entrainment causes a radially inward velocity in conjunction with the spatial acceleration of the jet. Small particles, those with smaller particle Stokes number, will better follow the mean gas motion which drives them to the spray centerline. Larger particles are less affected by the air entrainment and will follow more ballistic trajectories subject to initial velocity vectors arising from the jet breakup process and turbulent dispersion.

Farther downstream, the inward entrainment velocities are reduced to the point where smaller particles are substantially dispersed from the centerline. This is shown 810 mm downstream in Fig. 6 where the mean droplet diameter becomes more uniform.

The simulations capture the relative dispersion of the larger and smaller particles with good fidelity, both in the early development where the segregation process is strong and later when more uniform dispersion is predominant.

Also presented in Fig. 7 are the measured axial droplet velocities. These show the reduction in the particle velocity associated with the spreading of the spray and the transfer of momentum to the gas through drag forces. The water spray transfers momentum to the surrounding air and induces a flow, determined from the computational results, with Reynolds numbers on the order of 10^5. The air near the spray centerline is accelerated substantially more than that near the spray edge so that the outer droplets experience greater continuous drag and are slower. The measurements are compared with the simulated droplet velocities in Fig. 7. While the general agreement is good, there are certain characteristics of the predicted velocity profiles, at least at 480 mm, that indicate points of concern when collecting statistics using the present stochastic-separated flow approach. Of specific concern is collection of relatively large particles into a single parcel. Large particles are relatively rare, but they have a large Stokes number. The large Stokes number means that they easily reach the outer regions of the jet with substantial momentum; these large particles are the cause of the greater particle velocities at the edge of the spray, relative to the measured values. Because the SSF model transports large particles as a group, their effect is magnified. Increasing the total number of parcels, and thus reducing the particles per parcel will tend to ameliorate this effect, but there will always be a region near the edge of the spray where statistical uncertainty increases in association with a reduced number of parcels reaching that region. In Fig. 8, the snapshots of the spray are shown. Relatively large droplets are formed as the flow evolves downstream due to coalescence events. The contour color is scaled in Fig. 8 based on the droplet axial speed. It is shown that the droplet speed is reduced in the downstream direction due to drag.

Fig. 9 illustrates the time-averaged gas-phase velocity field in a plane through the jet centerline, with a superimposed contour plot indicating the relative particle number density. The gas is ini-

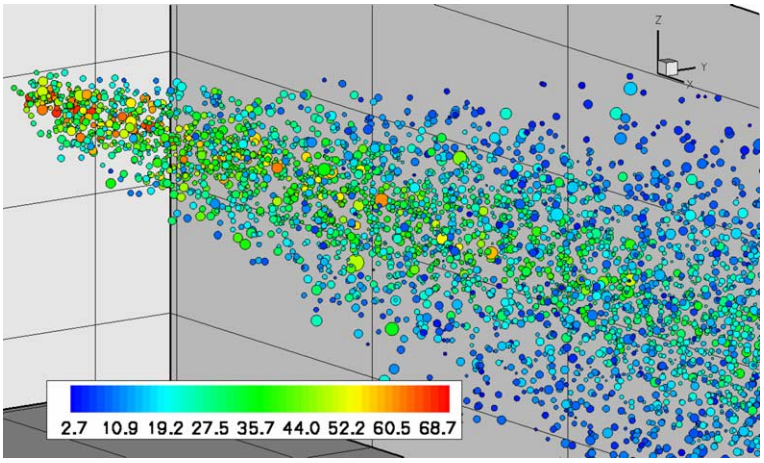

Fig. 8. Instantaneous snapshot of spray calculation at $t = 1.0\,\mathrm{s}$ using Hybrid collision model. Contour color indicates droplet axial speed in [m/s]. Symbol diameter is proportional to droplet diameter.

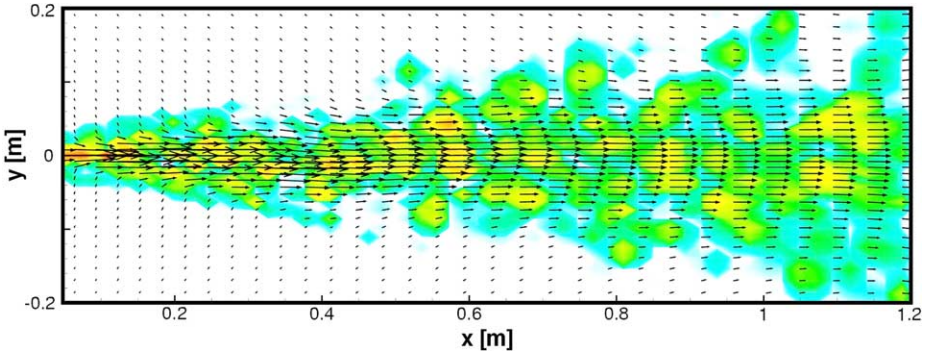

Fig. 9. Gas velocity vectors in the $z = 0$ plane, indicating centrally-directed entrainment. Superimposed contours indicate the local particle number density.

tially accelerated through aerodynamic drag interaction with the spray droplets, which decelerate and give up part of their momentum. Both the initial cone angle of the spray and the turbulent mixing of the accelerated air with the slower-moving air outside the spray are responsible for the widening of the velocity profile at downstream locations. The inward-directed velocity vector at the edges of the spray will certainly influence the smaller particles, which have a smaller aerodynamic velocity relaxation time (Crowe et al., 1998). These smaller particles will be preferentially swept toward the centerline of the spray, which may partially explain the previously observed increase in mean droplet size in the radial direction.

5.2. Grid sensitivity analysis

All simulations are run for $t = 2.0\,\mathrm{s}$, with time-averaged statistics being gathered from $t = 0.2\,\mathrm{s}$ up to $t = 2.0\,\mathrm{s}$. The interval between samples is $\Delta t_{\mathrm{stat}} = 0.0002\,\mathrm{s}$, so that all statistics are based on

9000 realizations. The computational domain size extends $1.2\,\mathrm{m} \times 0.8\,\mathrm{m} \times 0.8\,\mathrm{m}$, and a nonuniform grid is used to provide enhanced resolution near the spray. Three resolutions are tested, including a coarse grid of $42 \times 33 \times 33$, a medium grid of $52 \times 43 \times 43$, and a fine grid of $67 \times 53 \times 53$. Results for the medium and fine grid resolutions are similar enough to be deemed essentially grid-independent, and so the medium resolution is used for all subsequent work to keep simulation costs affordable.

5.3. Effect of evaporation model

In Fig. 10, droplet size distribution results are shown for both an evaporating spray and a non-evaporating spray at axial locations of $x = 480\,\mathrm{mm}$ and $x = 810\,\mathrm{mm}$. The overall size distribution trends are unchanged at both axial stations, although a counterintuitive increase in mean droplet size is observed in the outer portions of the spray at $x = 480\,\mathrm{mm}$. Close inspection of the simulation results indicate that this is attributed to the complete evaporation of a large number of initially small droplets, which biases the overall average toward the larger droplets.

5.4. Effect of collision model

Some limitations of the O'Rourke collision model have been reported (Ko et al., 2003). Collision probability in the O'Rourke model is somewhat mesh-dependent. In addition, the model ignores the preferred directional effects of droplets, and thus collision-criterion detects too many collisions. In the current case, overly frequent collision events yield overly predicted droplet size as

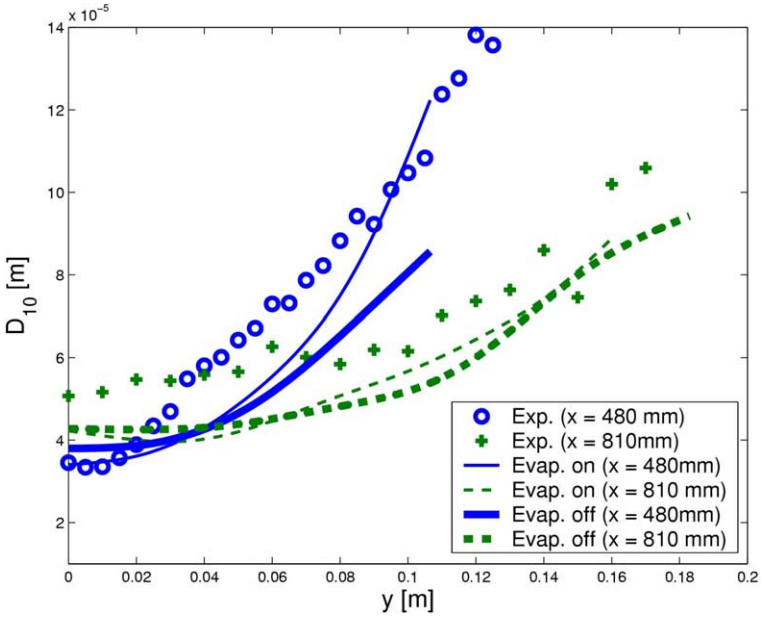

Fig. 10. Effect of evaporation model.

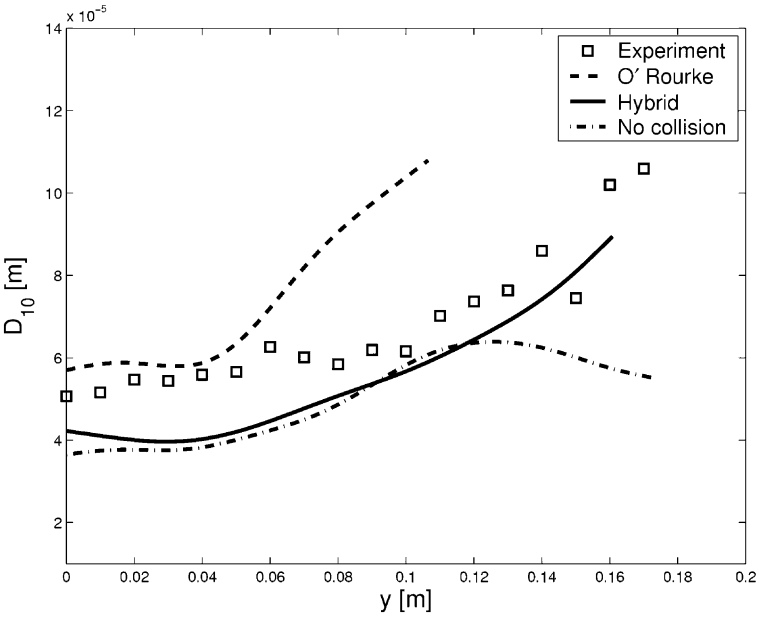

Fig. 11. Effect of collision models. Comparison is made at $x = 810$ mm.

shown in Fig. 11. For that reason, the Hybrid-model, which accounts for the preferred directional effects, is chosen for the current simulation. Mean droplet size profiles both with and without the use of the Hybrid collision model are also shown in Fig. 11. The droplet size result with the collision model is slightly larger than that without the collision model. However, the collision effect does not seem to be dominant. When the Hybrid collision model is used, moderate number of coalescence event occurs in a way so that the overall droplet size is not over-predicted. Some divergence behavior is observed at $x = 810$ mm; larger droplets due to coalescence are better capable of penetrating outwardly and thus relatively larger droplet size is seen for the collision model result. This phenomenon indicates that the collision does play some role in characterizing the droplet size distribution over the domain, even though the collision does not seem to have the dominant effect for this particular turbulent spray.

Reasonable success has been obtained in matching the simulation results with the experimental measurements using spray data at $x = 48$ mm as initial conditions. This, unfortunately, neglects the dynamics of the near-field portions of the spray. To ascertain the possibility of using the Rosin–Rammler distribution as an initial condition at the nozzle location, another simulation is performed where the initial conditions at the spray nozzle are set using the data at $x = 48$ mm, averaged over all radial locations. The experimental data from Fig. 4 is used, yielding a mean droplet size of $D_{10} = 40\,\mu$m and Rosin–Rammler model parameters of $X = 45\,\mu$m and $q = 1.5$. Starting at the nozzle, the spray evolves over the distance that would normally comprise the liquid core breakup and the dense-spray region. The complicated physics occurring within these regions are neglected except for the fact that the droplet collision model plays a significant role in this region. Simulation results using these initial conditions are shown in Fig. 12. While the overall agreement is still fairly good, there is evidence along the centerline at all downstream

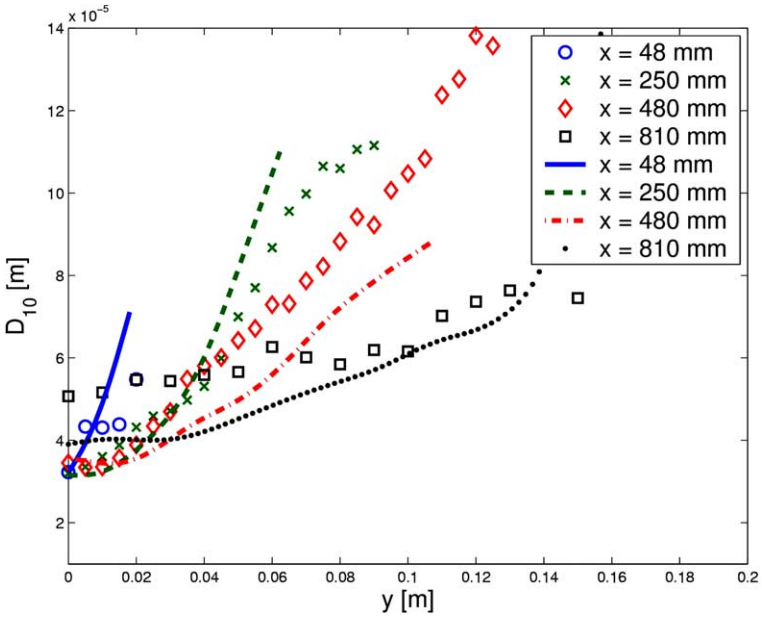

Fig. 12. Single-point injection using the extrapolated initial droplet size at $x = 0$ mm. Symbols are experimental data and lines are the computational results.

locations, including at 48 mm, that droplet collisions occurring in the first 48 mm of the simulation result in a somewhat different droplet size distribution. This highlights the difficulty of extrapolating back to the nozzle location using measurements from a short distance downstream: the nonlinear nature of the collision process for an expanding spray makes is difficult, though perhaps not impossible, to predict how the spray distribution will evolve without an iterative procedure. Because of the satisfactory results obtained using the measured droplet distributions at 48 mm downstream, we have elected not to pursue such a procedure at the present time.

6. Conclusions

A turbulent water spray is simulated using a stochastic separated flow technique that includes sub-models for droplet dynamics, heat and mass transfer due to evaporation, and collisions with possible coalescence. The semi-empirical prescription of initial droplet sizes and velocities used in this study is a novel Monte Carlo sampling technique using a prescribed Rosin–Rammler distribution that is parameterized in terms of experimentally measured arithmetic and Sauter-mean diameters. The computational results are compared to the experimental measurements, yielding the following observations:

(i) The dispersion coefficient (q) in the Rosin–Rammler distribution increases as radial location increases, indicating a more symmetric and uniform size distribution. The coefficient range near the nozzle exit (i.e. $x = 48$ mm) is about $1.40 < q < 2.65$.

(ii) A gradation of particle sizes in the radial direction occurs due to different dynamic behavior of small and large particles. Large particles are dispersed by the spray initial cone angle and subsequent interactions with turbulent eddies in the entrained air, while smaller particles are generally swept toward the spray centerline by aerodynamic drag interactions with the entrained air.
(iii) The droplet size distribution becomes more uniform downstream because most flow mechanisms (such as turbulent mixing and coalescence) approach statistical quasi-steady state.
(iv) Small particles do not have enough momentum to travel a large distance and thus only large particles exist in downstream locations.
(v) While evaporation does not play a major role at upstream locations, its effect is relatively significant at downstream and larger radial locations because droplets are exposed to a drier environment in the dilute spray region.
(vi) The effect of coalescence is not negligible and has a moderate role in characterizing the droplet distribution, especially in trends of droplet size and velocity at larger radial locations.

Acknowledgment

Sandia is a multiprogram laboratory operated by Sandia Corporation, a Lockheed Martin Company for the United States Department of Energy's National Nuclear Security Administration under contract DE-AC04-94AL85000.

References

Babinsky, E., Sojka, P.E., 2002. Modeling drop size distributions. Prog. Egy. Combustion Sci. 28, 303–329.
Bergwerk, W., 1959. Flow patterns in diesel nozzle spray holes. Proceedings of the Institution of Mechanical Engineers 173, 655.
Crowe, C., Sommerfeld, M., Tsuji, Y., 1998. Multiphase Flows with Droplets and Particles. CRC Press.
DesJardin, P.E., Gritzo, L.A., 2002. A dilute spray model for fire simulations: formulation, usage and benchmark problems, Sandia National Laboratories Technical Report, No. SAND2002-3419, Albuquerque.
Didonato, A.R., Morris Jr., A.H., 1986. Computation of the incomplete gamma function ratios and their inverse. ACM Transactions on Mathematical Software 12, 377–393.
Faeth, G.M., 1983. Evaporation and combustion in sprays. Prog. Egy. Combustion Sci. 9, 1–76.
Faeth, G.M., 1987. Mixing, transport and combustion in sprays. Prog. Egy. Combustion Sci. 13, 293–345.
Georjon, T.L., Reitz, R.D., 1999. A drop-shattering collision model for multidimensional spray computations. Atomization and Sprays 9, 231–254.
Gosman, A.D., Ioannides, E., 1981. Aspects of computer simulation of liquid-fueled combustion. AIAA Journal 81, 0323.
Hoyt, J.W., Taylor, J.J., 1977a. Waves on water jets. Jr of Fluid Mech 83, 119.
Hoyt, J.W., Taylor, J.J., 1977b. Turbulence structure in a water jet discharging in air. Phys Fluids 20, S253–S257.
Jones, W.P., Launder, B.E., 1972. The prediction of laminarization with a two-equation model of turbulence. Int. Jr Heat Mass Trans 15, 301–314.
Ko, G.H., Lee, S.H., Ryou, H.S., Choi, Y.K., 2003. Development and assessment of a hybrid droplet collision model for two impinging sprays. Atomization and Sprays 13, 251–272.

Maxey, M.R., Riley, J.J., 1983. Equation of motion for a small rigid sphere in a non-uniform flow. Phys Fluids 26, 883–889.

McCarthy, M.J., Molloy, N.A., 1974. Review of stability of liquid jets and the influence of nozzle design. Chem Eng Jr 7, 1–20.

O'Rourke, P.J., Amsden, A.A., 1987. The TAB method for numerical calculation of spray droplet breakup, SAE Technical Paper, 872089.

Pai, G.M., Subramaniam, S., 2004. Analysis of turbulence models in Lagrangian–Eulerian spray computations, ILASS-Americas, 17th Annual Conference on Liquid Atomization and Spray Systems, Arlington, VA, May.

Patankar, S.V., 1980. Numerical Heat Transfer and Fluid Flow. Taylor & Francis, New York.

Pope, S.B., 1978. An explanation of the turbulent round-jet/plane-jet anomaly. AIAA Journal 16, 279–281.

Press, W.H., Teukolsky, S.A., Vetterling, W.T., Flannery, B.P., 1992. Numerical Recipes in FORTRAN, The Art of Scientific Computing. Cambridge University Press, New York.

Ranz, W.E., Marshall, W.R., 1952a. Evaporation from drops: part I. Chem. Eng. Prog. 48, 141–146.

Ranz, W.E., Marshall, W.R., 1952b. Evaporation from drops: part II. Chem. Eng. Prog. 48, 173–180.

Rayleigh, W.S., 1878. On the instability of jets. Proceedings of the London Mathematical Society 10, 4.

Reitz, R.D., 1978. Atomization and other breakup regimes of a liquid jet, Ph.D. thesis, AMS Department, Princeton University.

Reitz, R.D., Bracco, F.V., 1982. Mechanism of atomization of a liquid jet. Phys Fluids 25, 1730–1742.

Sallam, K.A., Faeth, G.M., 1999. Drop formation at the surface of plane turbulent liquid jets in still gases. Int. Jr Multiphase Flow 25, 1161–1180.

Sallam, K.A., Dai, Z., Faeth, G.M., 2002. Liquid breakup at the surface of turbulent round liquid jets in still gases. Int. Jr Multiphase Flow 28, 427–449.

Shuen, J.S., Chen, L.D., Faeth, G.M., 1983. Evaluation of a stochastic model of particle dispersion in a turbulent round jet. AIChE Journal 29, 167–170.

Sterling, A.M., Sleicher, C.A., 1975. The instability of capillary jets. Jr Fluid Mech 68, 477–495.

Weber, C., 1931. Zum zerfall eines flussigkeitsstrahles. Zeitschrift Fur Angewandte Mathematik Und Mechanik 11, 138–145.

Widmann, J.F., Sheppard, D.T., Lueptow, R.M., 2001. Non-intrusive measurements in fire sprinkler sprays. Fire Tech. 37, 297–315.

Wu, K.J., Reitz, R.D., Bracco, F.V., 1986. Measurements of drop size at the spray edge near the nozzle in atomizing liquid jets. Phys Fluids 29, 941–951.

Wu, P.K., Ruff, G.A., Faeth, G.M., 1991. Primary breakup in liquid–gas mixing layers. Atomization and Sprays 1, 421–440.

Wu, P.K., Tseng, L.K., Faeth, G.M., 1992. Primary breakup in liquid–gas mixing layers for turbulent liquids. Atomization and Sprays 2, 295–317.

Yoon, S.S., Heister, S.D., 2003. Categorizing linear theories for atomizing round jets. Atomization and Sprays 13, 499–516.

Yoon, S.S., Heister, S.D., 2004a. A nonlinear atomization model based on a boundary layer instability mechanism. Phys Fluids 16, 47–61.

Yoon, S.S., Heister, S.D., 2004b. A fully nonlinear model for atomization of high-speed jets. Eng. Anal. Boundary Elements 28, 345–357.

Yoon, S.S., Hewson, J.C., DesJardin, P.E., Glaze, D.J., Black, A.R., Skaggs, R.R., 2004c. On the modeling of a solid-cone water spray, ILASS-Americas, 17th Annual Conference on Liquid Atomization and Spray Systems, Arlington, VA, May.

Zhou, A., Yao, S.C., 1992. Group modeling of impacting spray dynamics. Int. Jr Heat Mass Trans. 35, 121–129.